Polymorphism and Phase Control in Titanyl Phthalocyanine Thin Films Grown by Supersonic Molecular Beam Deposition†

Nicola Coppedè,‡ Tullio Toccoli,‡ Alessia Pallaoro,‡ Fabrizio Siviero,‡ Karsten Walzer,§ Marco Castriota,|| Enzo Cazzanelli,|| and Salvatore Iannotta*,‡

CNR/FBK Trento Division, Institute of Photonics and Nanotechnology, Via alla Cascata 56/C, Povo 38100 (TN), Italy, Institut fuer Angewandte Photophysik, George-Bähr-Strasse 1, 01069 Dresden, Germany, and LICRYL-INFM Laboratory-CEMIF.CAL, Department of Physics, University of Calabria, Via P. Bucci, Cubo 33B, 87036 Arcavacata da Rende (CS), Italy

Received: July 27, 2007; In Final Form: October 2, 2007

Polymorphism in the growth of titanyl phthalocyanine films on dielectric substrates has been systematically studied by UV absorption and micro-Raman analyses, correlating structure and optical properties. We explored different growth regimes as a function of substrate temperature and growth rate using hyperthermal seeded supersonic beams. We identify and discuss specific signatures in micro-Raman spectra specifically correlated to the different phases and demonstrate the unprecedented ability of growing crystalline films and controlling the relative abundance of the different phases (amorphous, phase I, and phase II) by the beam parameters. We envisage the very promising perspective of controlling polymorphism at low temperatures via supersonic beam growth, paving the way for better performing devices.

Introduction

Among π conjugated organic molecules, metal phthalocyanines (MPc) are widely studied because of appealing optical and electronic properties that, combined with their high thermal and chemical stability, make them interesting and promising candidates for applications in optoelectronic devices and gas sensors.[1] In particular, titanyl phthalocyanine (TiOPc) exhibits a wide absorption spectrum in the visible range, a large nonlinear optical susceptibility,[2] an ultrafast optical response, and a high photoconductivity.[3] Driven by these promising properties, an increasing interest has been devoted to exploit TiOPc as an active material in organic solar cells,[4,5] while applications in organic light emitting diodes and as a conducting layer in organic field effect transistors have been investigated.[6]

As MPc in general, TiOPc films are characterized by a strong polymorphism. Nevertheless, the peculiar nonplanar and polar structure gives rise to several crystalline phases, different from those typical of planar MPc. The main crystal structures of TiOPc, including the so-called phase I (also called β; monoclinic, with $P2_1/c$ space group and number of molecules per unit cell $Z = 4$), and phase II (also called α; triclinic, with $P1$ space group and $Z = 2$), have been identified by Hiller et al.[7] in the early 1980s by means of X-ray diffraction (XRD). Both phases are stable and can be grown as single crystals by CVD.[8] The existence of a third polymorph (phase Y) is also reported, and it is characterized by a crystal structure similar to phase I with a different tilt angle of the molecules in the $a-b$ plane. Phase Y has been grown in the form of powder or polycrystalline thin films, and its structure has been refined by Rietveld analysis and intermolecular energy minimization.[9] Besides XRD, the different TiOPc crystalline phases have been mainly characterized by absorption in the UV−vis region,[10,11] identifying features that are precisely and unambiguously associated with the different crystalline phases. A few papers also report Raman scattering studies,[12,13] where the first evidence of phase-dependent peak positions and intensities is discussed.

Analysis of crystalline structure and properties of thin films by absorption and Raman spectroscopies is a useful approach, especially advantageous for very thin films of titanyl phthalocyanine (which are difficult to characterize with XRD). Micro-Raman analysis is particularly valuable to study the formation and evolution of amorphous or crystalline regions, belonging to various phases, down to the micrometer length scale. Thus, the investigation of the film crystalline structure based on correlating data from UV−vis absorption and micro-Raman spectroscopies provides further insight into the polycrystalline structure of the films.

As is typical for many other organic molecules, optical and electronic properties of TiOPc thin films strongly depend on their structure and order. Therefore, the development of growth methods enabling appropriate control of the crystalline phase has crucial importance to fabricate devices with improved performances. Aiming at this purpose, several studies have been performed on the synthesis of TiOPc films. Among various techniques, the ones that give the best results are Langmuir−Blodgett (LB)[14] and organic molecular beam deposition (OMBD).[15] In the former case, phase II films were obtained by adding fatty acids or by exposing preformed films to solvents vapors, such as chlorobenzene or xylene. With regard to OMBD, several studies have addressed the influence of substrate temperature and deposition rate on the growth of different crystalline phases. These detailed investigations showed that, up to about 50 °C (on several different substrates including sapphire and PTFE), only amorphous films can be grown. By increasing the temperature in the range above 100 °C, the co-presence of amorphous and crystalline regions (phase I and

† Part of the "Giacinto Scoles Festschrift".

* Corresponding author. E-mail: iannotta@itc.it; fax: +39 0461 314875; tel.: +39 0461 314251.

‡ Institute of Photonics and Nanotechnology.

§ Institut fuer Angewandte Photophysik.

|| University of Calabria.

10.1021/jp075939m CCC: $37.00
Published on Web 11/14/2007

phase II) was observed. Even some degree of control on the majority phase has been achieved by tuning the deposition rate. At higher temperatures and on appropriate crystalline substrates (such as sapphire), films grow preferentially in phase II. A complementary approach to a selective production of films in phase I and phase Y is based on chemical postdeposition treatments, which consist of the exposure of the films to different solvents, such as chlorobenzene or xylene, and in annealing procedures.[16]

The present paper reports on supersonic molecular beam deposition (SuMBD) of TiOPc thin films on quartz, demonstrating and discussing the dependence of structural properties on substrate temperature and deposition rate and further exploring the ability to control the type of growth. In previous papers,[17,18] we have shown that kinetic energy supplied to the molecules by supersonic expansion has remarkable ordering effects on the morphology of TiOPc thin films grown on both ordered crystalline (mica) and amorphous (quartz) substrates. The major end result was nucleation of larger and higher quality crystals with respect to OMBD deposition. With the exploration of a range of deposition conditions, we show here that hyperthermal beams give unprecedented control on the growth, producing crystalline films with a controlled structure and different phases even at room temperature and on amorphous substrates, depending on the deposition rate. This is a remarkable result that further confirms the perspective of the SuMBD approach as a promising method for the synthesis of controlled organic functional films.

Experimental Procedures

Thin Film Growth. The growth of thin films has been performed in a tailor-made supersonic beam deposition apparatus, previously described in more detail.[19] It basically consists of a differentially pumped supersonic beam, a TOF mass spectrometer, and a deposition chamber. The supersonic beam source, placed in a high vacuum chamber, is made of a quartz tube closed at the front end, where a nozzle (typically 50−130 μm in diameter) is present. An inert carrier gas (helium in this experiment) is supplied to the source, where the organic material is sublimated by Joule heating and dispersed at very low concentrations into the gas expanding through the nozzle. By changing the working parameters (nature and pressure of the carrier gas, sublimation temperature, nozzle diameter, and temperature), we can finely control key properties of molecules in the supersonic beam such as kinetic energy, momentum, and degree of cooling of internal degrees of freedom typically induced by expansion.[20] The source was typically operated using a He carrier gas pressure in the range of 100−200 kPa. The central part of the beam was selected by skimming the free jet expansion via a sharp edged conical collimator, which separates the source from the deposition chambers (base pressure 10^{-8} mbar). Here, the molecular beam is intercepted by the substrate, the temperature of which can be varied from −115 up to 350 °C, with a stability of about ±1 °C.

The TiOPc films have been grown in a temperature range from 25 to 125 °C on amorphous quartz plates, the rms roughness of which is typically 1.5 nm, as measured by atomic force microscopy (AFM). A quartz microbalance measures the deposition rates. To assess the effects of the beam flux, we selected two quite different growth regimes: a high rate of 1.0 nm/min and a low rate of 0.05 nm/min. The source operating conditions have been tuned to keep the same high kinetic energy of 15 eV for all the films deposited. The in-line time-of-flight mass spectrometry (TOF-MS) coupled to laser (fourth harmonic of a Nd:YAG laser at 266 nm) multiphoton ionization monitors the intensity, purity, and stability of the beam. The duration of the deposition has been properly varied to produce films of the same thickness (∼20 nm) for both deposition rates. We used TiOPc row material coming from the same batch (Syntec-Sensient GmbH) for all experiments. We purified it by repeated vacuum gradient sublimation cycles, after which the TOF mass spectra did not show any significant residual contamination. We prepared also amorphous reference samples by a homemade evaporator operating under high vacuum conditions (10^{-7} mbar). We used the same TiOPc powder in a tantalum boat and the same quartz substrates, producing samples with a thickness up to 2 μm.

Characterization Techniques. We used a Nanoscope IIIa (Digital Instruments) AFM instrument in tapping mode to study the topography of the samples. The UV−vis spectra were collected by a Varian Cary 5000 spectrometer.

We carried out the Raman measurements by a microprobe setup (Horiba-Jobin-Yvon, model Labram) equipped with a CCD detector and a He−Ne laser (632.8 nm emission). In the following experiments, we used the highest resolution grating available with 1800 grooves/mm. We could estimate the resulting uncertainty of the peak position to be about 1 cm^{-1} for the narrow peaks and about 3 cm^{-1} for the broader bands. This experimental error is mainly due to the combined effect of the resolving power of the grating, the pixel size of the CCD, and the errors in the correction procedure of the drift in the monochromator frequency setting (performed by subtracting the apparent position of the laser line, monitored at regular time intervals).

Two objectives were used to collect the spectra: a 100× and a 50× long working distance. The laser power out of the 50× objective was about 5 mW, and the diameter of the focused spot was about 3−4 μm. Therefore, the irradiance for the unfiltered laser beam was of the order of 50 kW/cm^2. By using neutral filters of variable optical density (OD), the laser power impinging on the samples could be reduced to the following amounts: 50% for the OD 0.3 filter, 25% for OD 0.6, 10% for OD 1, and 1% for OD 2. Proper filters were chosen to have a good signal-to-noise-ratio without excessive heating: typically, an OD 0.6 filter was adopted with the 50× objective and an OD 1 filter with the 100× objective. A special X−Y stage for spectral mapping was used to point out and map the interesting zones of the samples.

Results

Morphology of TiOPc Thin Films. In previous publications,[17,18] we systematically studied the morphology of TiOPc films grown by SuMBD on quartz substrates. Quite different film morphologies were observed and characterized as a function of the growth conditions, in particular, substrate temperature. Two different main regimes were identified there: growth at temperatures up to 25 °C, where a rather non-textured morphology was observed, and higher substrate temperatures, leading to the growth of rough layers with the dominating presence of isolated crystals. Here, we only recall some of the major trends observed that have been confirmed by the present experiments. The crystal size depends strongly on the growth regime. In fact, the film roughness and height scales measured by tapping mode AFM results in being very different: the min−max height scale being14 nm (2 nm rms roughness) for films grown at room temperature and 60 nm (13 nm rms roughness) for films grown at high temperatures. The transition from homogeneously distributed flat grains to polycrystalline films is clearly visible and predictable. The crystallites within the polycrystalline film

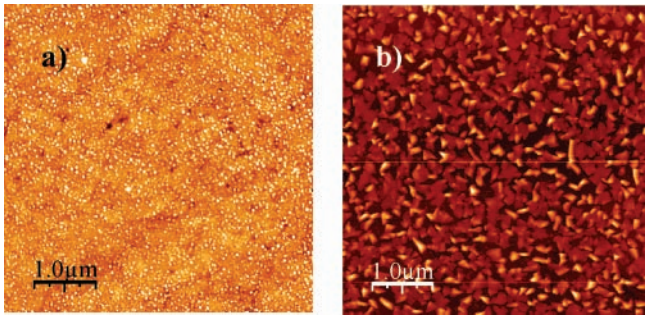

Figure 1. 5 μm $\times$ 5 μm AFM micrographs of TiOPc thin films deposited on quartz by SuMBD at a substrate temperature of (a) 25 °C and (b) 165 °C, respectively.

do not follow a preferred direction as one would expect in the growth on an amorphous substrate.

Figure 1 shows the typical morphologies observed by AFM on films that are representative of the two extremes of the temperature range explored in this work. The samples were grown at 25 and 165 °C, respectively, with a thickness very similar to all the other films grown at different substrate temperatures. The typical texture of room temperature grown samples is characterized by a uniform distribution of small grains, the lateral dimensions and height of which are typically smaller than 50 and 10 nm, respectively. At high temperatures, we observe the growth of much larger crystallites with well-defined different shapes. Between the grains, we have an indication of the presence of a wetting layer, as confirming precedent studies.[17] In fact, by comparing the roughness measured by AFM in regions between the crystallites and on the clean substrates, the presence of the wetting layer can be assessed. We therefore used a shadow mask during growth to characterize the same substrate. In fact, the high scale in the two zones resulted in being very different, being atomically flat on the shadowed region of the substrate and about 1.7 nm in between the crystallites. The Micro-Raman spectra also reveal the presence of TiOPc in the areas between larger grains, confirming the presence of a wetting layer.

UV−vis Absorption. The optical absorption spectrum of the TiOPc films was characterized by two main broad bands: a B Soret band in the near-UV and a Q band in the visible region. Both of them include different components whose positions and intensities are known to be sensitive to the specific crystalline phase. In particular, the Q band, ranging from about 550 to 900 nm, is characterized by at least two components, Q_x (at the low wavelength side) and Q_y (at the high wavelength side), that are due to HOMO−LUMO transitions. Their energy, according to Mizuguchi et al.,[11] is strongly influenced by molecular distortion induced by $\pi-\pi$ interactions between adjacent molecules along the *c* axis. As a consequence, the absorption properties in the visible range are very sensitive to the crystalline structure, which determines the degree of overlap between orbitals of neighboring molecules. Even though, as discussed in the following paragraphs, the literature is sometimes somewhat contradictory, mostly because of the different type and quality of the samples studied, the available literature[11,14,16] gives definitive information about the UV−vis absorbance spectroscopic signatures (fingerprints) of different crystalline phases. Amorphous films typically show Q_x and Q_y bands at 645−660 and 714−718 nm, respectively, while the main B band component is centered at 345−350 nm. Phase I films give rise to red-shifted Q_x and Q_y bands positioned at about 670 and 755−760 nm, respectively, with a B band main component at about 370 nm. Finally, phase II films show the highest separation between the Q bands, with

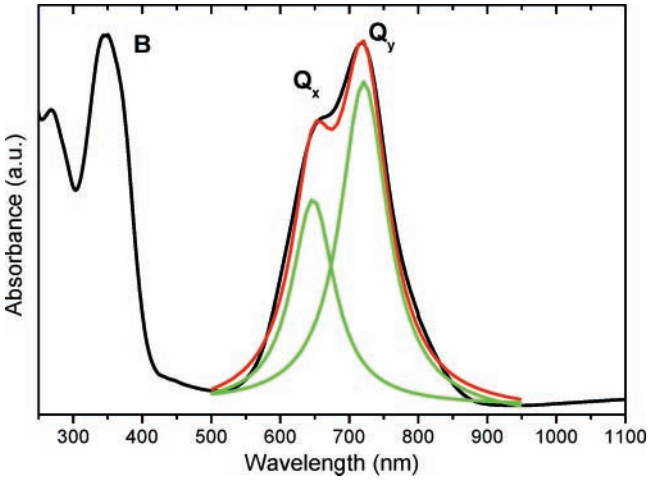

Figure 2. Optical absorption spectra of the TiOPc reference amorphous sample grown by OMBD; the Q_x, Q_y, and B bands are clearly visible and identified. The best fit of the Q bands is also plotted.

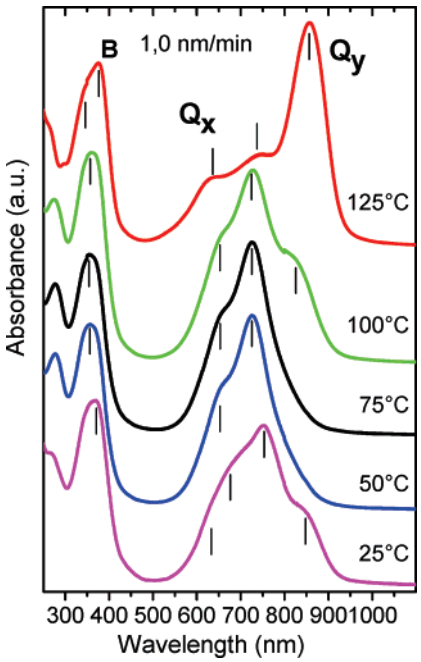

Figure 3. Optical absorption spectra of TiOPc thin films grown by SuMBD at the high rate (1.00 nm/min). The spectra are labeled with the different temperatures of the substrate at which the samples have been grown. The position of the Q and B band components, as calculated from a best fitting procedure (see Table 2), are indicated by short black lines. Q_x, Q_y, and B band positions are also labeled in the 125 °C spectra.

an even higher red-shift of the Q_y component, so that the positions of the Q_x and Q_y bands are typically at 630−635 and at 845−850 nm, respectively, while the B band main component is shifted at 375−380 nm.

Figure 2 shows the typical absorption spectrum of an amorphous film, grown in our lab by OMBD, where these major different features are clearly visible together with the best-fitted Q_x and Q_y components, centered at 657 and 716 nm, respectively.

Figure 3 shows the typical UV−vis absorption spectra of samples grown by SuMBD on different substrate temperatures ranging from 25 to 125 °C and at a deposition rate of about 1.0 nm/min (the high rate). The positions of the main absorption bands have been determined by fitting the spectra with Lorentzian lineshapes and are reported in Table 1. Already, at a first

TABLE 1: Wavelength Positions of Optical Absorption Bands of TiOPc Films Deposited by SuMBD on Quartz at High Rate and Low Rate[a]

		λ_{max} (nm)				
deposition rate	*T* (°C)	B band	Q band			
1.00 nm/min	125	378	634		739	855
	100	360	650		729	826(sh)
	75	356	649		728	
	50	356	651		728	
	25	370	631	670	757	851(sh)
0.05 nm/min	125	380	632		750	860
	100	362	642		719	834(sh)
	75	350	645		717	
	50	350	644		716	
	25	377	629	677	763	847

[a] Peak positions of Q band components have been obtained by best fitting the spectra, while only the observed maximum is reported for the B band.

comparison among the different spectra, it appears that there is a quite clear strong evolution, which is a definite indication of the different structure of the films.

Samples deposited at 125 °C give rise to spectra with typical signatures of phase II. We observed very similar spectra by SuMBD at temperatures up to 220 °C. The distinctive features are that the B band includes two components at about 345 and 380 nm, the second being clearly prominent, and the Q_x and Q_y bands are highly separated and positioned at 634 and 855 nm, respectively. The overall spectrum is very similar to that obtained by OMBD at $T > 100$ °C on single-crystal substrates.[14,15] Nonetheless, the Q_y band is enhanced and red-shifted by about 5−10 nm with respect to the spectra of phase II films obtained with vapor solvent treatments[11,16] by Mizuguchi et al. and Saito et al.

A similar trend of the Q_y bands, in terms of positions and intensity, has been observed in low temperature measurements and has been ascribed to a lattice contraction along the molecular stacking.[11] This is an indication that SuMBD deposited phase II crystals present a higher contraction along the *c* axis with respect to films of the same crystalline phase obtained by chemical routes.

Figure 3 also shows that the films deposited at 100 °C are characterized by quite different absorption spectra. There is the presence of features reminiscent of an amorphous phase, combined with a smaller component of phase I and with a marked shoulder at 826 nm, in a position typical of phase II crystals in chemically grown samples.[11] Here, the B and Q_y bands show a significant red-shift. In particular, the band at 729 nm results in being about 10 nm shifted with respect to the typical amorphous phase. Such a trend has been previously observed in SuMBD grown films,[17] in the same temperature range, and has been ascribed to the presence of a crystalline fraction, possibly in phase I. Further decreasing the temperature of growth (75 to −50 °C), the presence of this phase I feature is preserved with the main peak fixed at 728 nm, while the band at 855 nm, due to phase II, disappears (see Figure 3).

A much more interesting behavior is observed in the SuMBD deposition at room temperature. Here, the mentioned trend toward a dominant amorphous structure, as the temperature decreases, appears to be reversed and in clear contrast to OMBD studies.[14] In fact, we observe a very broad Q band, including typical components of phase I (Q_x at 670 nm and Q_y at 757 nm[16]) and extra shoulders at both high (631 nm) and low energies (851 nm), assignable to the presence of a phase II component. Moreover, the B band shows an enhancement of the component at higher wavelengths with respect to the characteristic band of the amorphous phase. However, the residual presence of a little amorphous fraction cannot be fully excluded on the basis of the absorption spectra alone.

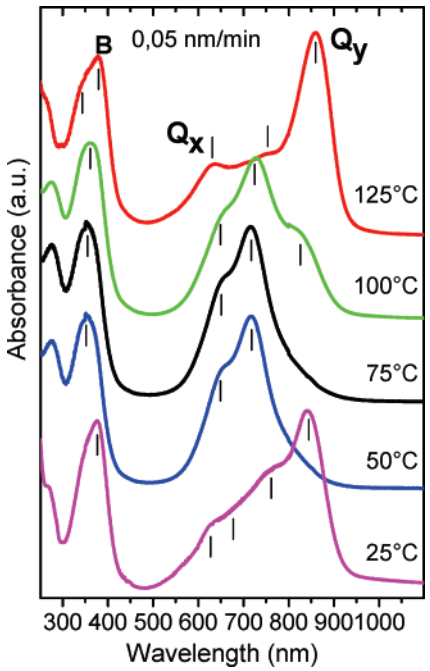

Figure 4. Optical absorption spectra of TiOPc films grown by SuMBD at the low rate (0.05 nm/min). The spectra are labeled with the different temperatures of the substrate at which the samples have been grown. The positions of the Q and B band components, as calculated from a best fitting procedure (see Table 2), are indicated by short black lines. Q_x, Q_y, and B band positions are also labeled in the 125 °C spectra.

Samples grown in the low rate regime show some relevant differences. Figure 4 shows the evolution of the absorption spectra versus substrate temperature for samples grown at the low rate (0.05 nm/min).

We observe minor but relevant changes in the spectra for films deposited at 125 °C. In fact, the Q_x and Q_y bands shift by a few nanometers toward lower and higher wavelengths, respectively (i.e., their separation increases) while the intensity of the Q_x band is enhanced. A similar trend, as a function of decreasing deposition rates, was observed also by Yamashita et al.[14] by OMBD. Films grown at 100 °C show an evident shoulder at 834 nm, possibly higher than in the high rate regime, indicating the presence of a significant fraction of phase II in the film.

For deposition temperatures ranging from 100 down to 50 °C, the spectra show typical fingerprints of an amorphous film. The main Q band for films grown at 75 and 50 °C in fact peaked at about 716 nm, which is the position typically observed for the amorphous phase.

Once again, the samples grown at 25 °C show spectra with major differences with respect to both OMBD and high rate (1.0 nm/min) growths. The typical spectrum (see Figure 4) is characterized much more clearly by features typical of phase II growth, as the intense B band at 377 nm and the Q bands at 629 and 847 nm. The position of the Q_y band, shifted at 847 nm, is an indication of a lower lattice contraction along the molecular stack with respect to the phase II samples grown at high temperatures. Nonetheless, there are also indications of the presence of minor components of other phases. In fact, the intensity of the Q band shows an enhancement in the 600−800 nm region with respect to the typical phase II, a feature that is compatible with the presence of small portions of phase I.

TABLE 2: Wavelength Peak Positions of Selected Raman Spectra of TiOPc Films Deposited by SuMBD and Shown in Figure 6[a]

1.00 nm/min			0.05 nm/min			
Raman shift (cm^{-1})						
substrate temp (°C)						
125	75	25	125	75	25	assignment
	1529			1529		pyrrole stretch
1515	1513	1511	1515	1512	1513	pyrrole stretch, a_1
1453	1450	1457	1452	1450	1450	isoindole stretch
1437	1433	1432	1435	1433	1434	isoindole stretch, a_1
1346	1341	1345	1341	1342	1341	pyrrole stretch, a_1
1305	1304	1305	1306	1304	1305	C−H bend
1210	1209	1211	1210	1210	1210	C−H bend
1196	1192	1187	1196	1192	1196	C−H bend
1146	1142	1148	1142	1141	1143	pyrrole ring breathing
1107	1105	1111	1106	1104	1106	C−H bend
940	947	938	940	949	940	TiO stretch
838	831	840/834	836	828	839	macrocycle stretching, a_1
751	748	750	750	749	752	macrocycle stretching, e
679	680	678	679	680	680	macrocycle breathing, a_1

[a] Two different SuMBD growth rate regimes are listed. Assignment to vibrational modes is based on Jennings et al.'s[12] deposition rate.

Micro-Raman Analysis. We carried out a systematic study of the local structure of the films to better understand their crystalline composition, complementing the information obtained by UV−vis absorption measurements. Several series of spectra have been acquired in several different positions for each sample, to investigate the presence of the different microcrystalline phases. Table 2 lists the main peaks observed in our experiments and their assignments to the molecular vibrational modes, based on the procedure reported in ref 12. In particular, the spectral features above 1000 cm^{-1} are associated with pyrrole, isoindole, and C−H vibrational modes, while the features in the 650−850 cm^{-1} region are due to macrocycle vibrations. The position of the pyrrole stretching peak in the region 1505−1530 cm^{-1} is very sensitive to the crystalline structure. Furthermore, since the HOMO−LUMO levels are located on the macrocycle of the phthalocyanine molecules,[21] we also expect that the Raman intensity of the modes below 1000 cm^{-1} is sensitive to the crystalline phase, as observed for the Q bands in the UV−visible spectra. Indeed, when an excitation line close to the Q absorption band is used, an enhancement of the Raman signal intensity from that spectral region is observed, due to a Raman resonant effect. In this way, we could study in much more detail the macrocycle vibrational modes, gaining better insight as compared to previous studies.

We first characterized by micro-Raman analysis the film grown by OMBD that we believed to be a typical amorphous film, on the basis of the corresponding UV−vis spectrum that is reported in Figure 2. The micro-Raman spectrum (see Figure 5) of this type of film shows, in fact, together with the typical features associated with amorphous films, the presence of a small contribution of Raman peaks typical of crystalline phases. In fact, in the pyrrole stretching peak, two components can be resolved, the stronger one generally assigned to an amorphous film, between 1528 and 1531 cm^{-1}, and the other, much less intense, at 1511−1513 cm^{-1}, typical of a crystalline structure. A very similar pattern is observed in the TiO stretching mode, where together with a main peak at 948−950 cm^{-1} (amorphous character), a smaller feature appears at 939−940 cm^{-1} (crystalline character).

In general, on the basis of our extensive experimental data, comparing many different spectra on a wide number of samples, we associate the amorphous phase with the following distinctive features in the Raman spectra line shapes. The first signature is the frequency position of the different modes: the pyrrole stretching mode lies in the range of 1528−1531 cm^{-1}, while the TiO stretching is in the range of 948−950 cm^{-1}. A second signature comes from the intensity ratios: a much lower intensity is generally observed in the macrocycle breathing mode (680 cm^{-1}) with respect to the pyrrole stretching band. Furthermore, the lower frequency isoindole stretching mode at 1434 cm^{-1} is much weaker than the one at higher frequency (1450 cm^{-1}). A final very relevant feature is the fwhm that is significantly larger for many of the peaks for the amorphous phase. In particular, the peak due to the macrocycle breathing mode, being isolated and well resolved, allows for the best quantitative evaluation of this parameter.

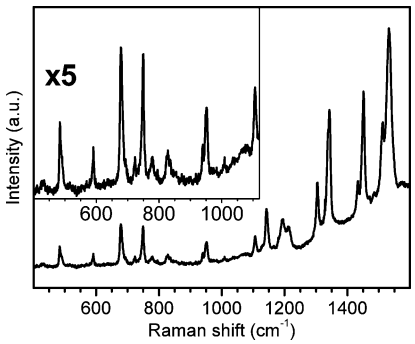

Figure 5. Micro-Raman spectra of the TiOPc amorphous (reference) sample grown by vacuum evaporation on a quartz substrate.

Such features, typical of the amorphous phase, have been systematically observed in our micro-Raman study even though a purely amorphous film could not be easily prepared. In fact, the frequent observation of the weak Raman peaks at 1511−1513 and 939−940 cm^{-1}, present even in the amorphous reference samples, is an indication of the presence of a small crystalline fraction (see Figure 5). Likewise and symmetrically, even the best crystalline films reveal from micro-Raman investigation traces of different phases, including amorphous phases. In the following paragraphs, the discussion will hence focus on the strongly dominant features observed in the films.

Figure 6 shows the evolution of the Raman spectra of SuMBD grown films, as a function of substrate temperature and deposition rate. We show two typical sets of data for films grown at high rate (1.00 nm/min) and low rate (0.05 nm/min) at the same three temperatures: 125, 75, and 25 °C. The spectra are by far representative of the most abundant spectral features observed in the corresponding films.

The samples prepared at 125 °C show a uniform crystalline structure on the microscale. The Raman spectra for high and low deposition rates are very similar, as already observed for the corresponding absorption spectra (see Figures 3 and 4). The pyrrole stretching peak is centered at 1515 cm^{-1}, which is in the range generally assigned to phase II,[12] hence confirming the UV−vis characterization of these samples. The very weak shoulder at 1530 cm^{-1} reveals the presence of quite a small fraction of the amorphous phase (more pronounced in samples grown at low rate), an aspect that could not be observed in the absorption spectra. The macrocycle modes give rise to a strong breathing band at 678 cm^{-1}, the intensity of which is higher than the pyrrole stretching at 1515 cm^{-1}. Three other bands are well-defined at higher energies (respectively, at 751, 838, and 940 cm^{-1}) near the macrocycle breathing peaks, showing similar intensities, among which lies the TiO stretching mode, at 940 cm^{-1}. This overall spectral profile results to be distinctive of phase II crystals, as it will become even more evident in the

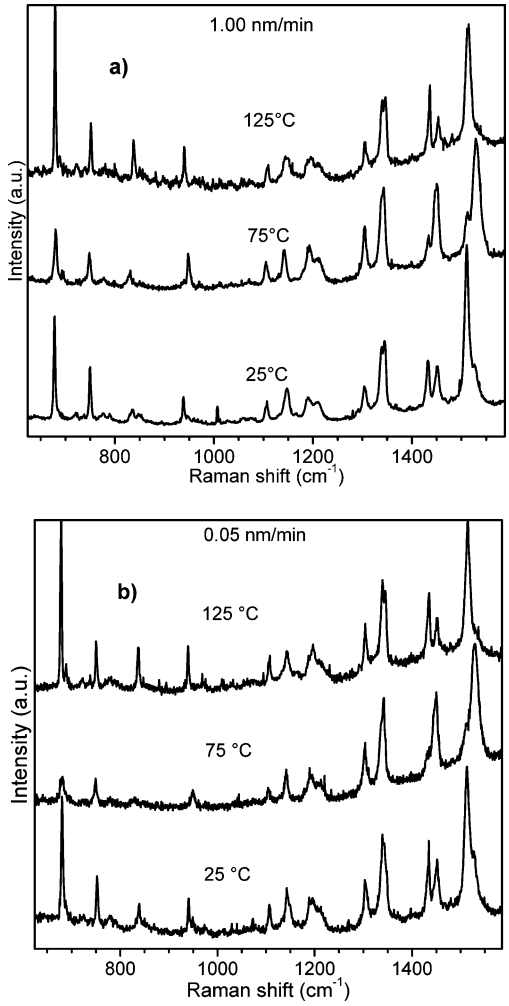

Figure 6. Selected typical micro-Raman spectra of TiOPc films deposited at different substrate temperatures. (a) Films grown at the high rate of 1.00 nm/min and (b) films grown at the low rate of 0.05 nm/min.

following, when we will compare with the Raman spectra typical of different crystalline structures.

TiOPc samples grown at lower substrate temperatures (75 and 50 °C) also show a rather uniform structure, somewhat insensitive to the deposition rate. In fact, no significant variations in peak positions are observed among samples grown with different deposition rates. As shown in Figure 6, the typical spectra for films grown at 75 °C exhibit TiO and pyrrole stretching peaks at 950 and 1529 cm^{-1}, respectively, following the typical pattern of an amorphous structure, while the shoulder at 1513 cm^{-1} suggests the presence of a minor crystalline component in the films. This feature is consistent with the evidence of a red-shift of the Q_y component observed in the absorption spectra (see Figure 3), of samples deposited at high rates. It, therefore, confirms the presence of a minor crystalline fraction, while the relative intensity of the macrocycle modes is coherent with a prevalent amorphous phase. Indeed, as observed for amorphous reference samples, the intensity of the peaks in the 450−850 cm^{-1} region is strongly depleted with respect to crystalline films. From this point of view, there is a significant difference between the two rates of deposition since the high rate grown films show better defined and higher peaks, indicating a trend toward a better crystalline order.

Another interesting Raman feature, discriminating amorphous from crystalline phases, emerges from our detailed studies. It is the relative intensity of the two nearby peaks centered at about 1434 and 1450 cm^{-1}. In amorphous films (see Figures 5 and 6), the peak at 1450 cm^{-1} is by far the dominant feature, the other appearing just as a sort of shoulder. This occurs systematically in our amorphous reference samples and is observable in the spectra of previous studies.[12] In good crystalline samples, the two peaks become of comparable intensity and well-resolved.

Considerations similar to those made for the samples grown at 75 and 50 °C hold for films deposited at 100 °C. The only significant difference is a much better defined shoulder at 1514 cm^{-1}, which is consistent with the presence of a larger crystalline fraction of phase II as also supported by the mentioned existence of a low energy component in the UV−vis absorption spectra (see Figures 3 and 4).

The samples grown at room temperature (25 °C) show a lower degree of uniformity on the microscale, with a coexistence of different crystalline phases in a proportion that is controlled by the deposition rate. In the samples grown at high rate, two different overall Raman spectral patterns have been observed. The first one, which is the most recurrent one, is shown in Figure 6a. Here, the pyrrole stretching mode is located between 1510 and 1511 cm^{-1}, the TiO stretching lies at 938 cm^{-1}, while the peaks at 678 and 750 cm^{-1} dominate the region below 1000 cm^{-1}. A small shoulder at 1528 cm^{-1}, indicating the residual presence of an amorphous fraction, is also observed. In the other group of spectra, the pyrrole stretching mode is shifted in the 1512−1514 cm^{-1} range (still with a small contribution due to the amorphous phase at 1530 cm^{-1}). The macrocycle modes show typical features of phase II (i.e., quite similar intensities of the three modes between 680 and 1000 cm^{-1}).

On the basis of observations by Jennings et al.,[12] who reported the occurrence of a peak at 1509 cm^{-1}, one could assign the first type of spectra to crystalline phase Y. In our SuMBD grown samples, this would be in clear contrast to the UV−vis spectra. Indeed, the typical Q band of phase Y crystals[12] should occur at 800−810 nm, which is too far from the 757 nm intense band observed in our absorption spectra (see Figure 3). As previously discussed, this is the typical signature of phase I and is also consistent with the majority of the Raman signatures observed as being characteristic of phase I.

Let us discuss now the low rate growth on room temperature substrates. The large majority of the collected spectra exhibit typical features of phase II (Figure 6b): the pyrrole stretching peak lies at 1514 cm^{-1}, the peak at 680 cm^{-1} has intensity comparable to that of the pyrrole stretching mode, and it is followed by three peaks with similar intensities. Nevertheless, in a few positions over the sample, Raman spectra with the characteristic shape of phase I were found, very similar to the one reported at the bottom of Figure 6a.

It is worth summarizing for the films grown by SuMBD on a room temperature substrate the overall indications coming from both Raman and absorption spectra. They all show a highly predominant microcrystalline character, with a relative abundance between phase I and phase II that is controlled by the deposition rate: a high deposition rates favors phase I growth and vice versa.

Discussion

According to Mizuguchi et al.,[11] the splitting between the Q_x and the Q_y bands in the absorption spectra of TiOPc films is due to the molecular distortion induced by the $\pi-\pi^*$ interaction between adjacent molecules along the *c* axis. The effect is a change in molecular symmetry from C_{4v} to C_1 in the solid state. The double degeneracy of the LUMO state in C_{4v} symmetry is

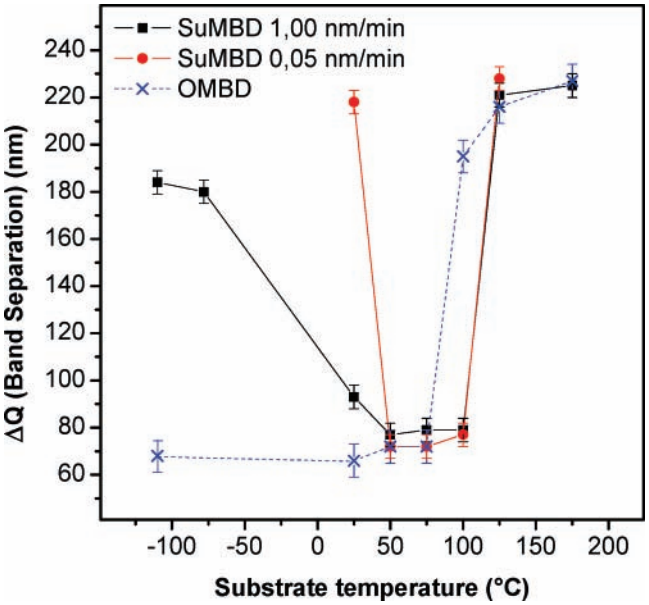

Figure 7. Plot of the splitting ΔQ, between Q_x and Q_y bands in the UV−vis spectra of TiOPc films, as a function of substrate temperature during growth. The data for samples grown with OMBD have been extracted from the work by Yamashita et al.[14]

removed, and hence, the single optical absorption band corresponding to the HOMO−LUMO $\pi-\pi^*$ transition splits into Q_x and Q_y components, the separation of which is larger as the molecular distortion increases. The highest separation is hence expected for crystalline phase II, and then it progressively decreases for phase I and for amorphous structures. To better compare with OMBD growth,[14] we now analyze in terms of the Q band splitting ($\Delta Q = Q_y - Q_x$) observed between the most intense components of the absorption spectra (Figures 3 and 4). This will shade some further light on the scenario coming out of TiOPc thin films deposited by supersonic molecular beams.

Figure 7 shows ΔQ for SuMBD grown films as a function of substrate temperatures and compared to the corresponding OMBD data reported by Yamashita et al.[14] (confirmed in our lab), where the TiOPc films grown by OMBD were deposited on sapphire crystals at a rate of 0.2−0.5 nm/min. As a supplement of information, in the figure, we have also included data coming from SuMBD samples deposited at low temperature, a detailed discussion of which has been previously published.[17] SuMBD deposition at high temperatures (≥125 °C) leads to films with high ΔQ splittings, very similar to those of OMBD samples and typical of the polycrystalline phase II. In SuMBD, lowering the temperature of growth to 100 °C causes already an abrupt change in the film structure. The dominant component becomes amorphous and hence characterized by much smaller ΔQ bands splitting. The residual fraction of phase II disappears as the temperature is brought down to 75 and 50 °C.

Films deposited by OMBD at 100 °C maintain instead a substantial crystalline character that is depleted only at lower temperatures so that amorphous films are obtained at substrate temperatures around and below 75 °C. Brinkmann et al.[15] have reported analogous results for depositions on PTFE substrates.

However, the major result of our study comes from the differences observed in the depositions at room temperature. Here, OMBD shows a ΔQ becoming even smaller, hence confirming a trend toward films with increasingly amorphous character for decreasing temperature. Exactly the opposite behavior is observed in SuMBD growth. Indeed, these films exhibit a substantially crystalline structure, with a separation between the main Q bands that are those typical of the phase I and phase II polymorphs, depending on the growth rate used. A further enhancement of the splitting is observed for SuMBD deposition at lower temperatures, confirming the peculiar tendency toward the development of crystalline structure for temperatures below 25 °C.

A quantitative analysis of the micro-Raman spectra gives information that further confirms this rather peculiar trend in the structural order of SuMBD grown TiOPc films. We introduce two parameters that quantify the high sensitivity of Raman features to the crystalline order: (i) the fwhm of the macrocycle breathing mode (MBM) and (ii) the intensity ratio between the pyrrole stretching peaks that is, as already mentioned, between the one typical of crystalline phases (A_C) and the other associated to the amorphous structures (A_A). This choice was guided by the fact that the width of Raman peaks, at a fixed temperature, is inversely correlated with a crystalline order that is very sensitive to grain size and density of defects. In particular, we choose the line width of MBM, at about 680 cm^{-1}, for its rather high intensity in all the spectra and for the absence of shoulders that would complicate the width measurement. Its fwhm has been averaged over a full series of micro-Raman spectra collected in different spots for each sample. On the other hand, the A_C/A_A parameter provides an indication of the relative fraction of amorphous phase in the films. It has been calculated as the ratio between the areas of the pyrrole stretching peaks in the 1510−1515 cm^{-1} region (crystalline phase) and in the 1528−1531 cm^{-1} region (amorphous phase). The two contributions have been separated by a line-shape fitting procedure, and the areas have been summed among the whole series of collected spectra for each sample.

Figure 8a,b shows the evolution of these two parameters as a function of the substrate temperature, comparing the high rate and low rate regimes of SuMBD growth. Both the plots (MBM fwhm in Figure 8a and A_C/A_A in Figure 8b) show the same general trends. When the substrate temperature decreases down to about 60−70 °C, the observed trends are consistent with an increase of disorder and defects as well as of the amorphous fraction in the deposited films. This tendency is clearly reversed below 50 °C down to room temperature.

The plots of Figure 8 give also further interesting information about the ability of controlling the growth in terms of crystalline quality and relative abundance of the amorphous phase. For example, in the growth at 100 °C, lower growth rates give a larger fraction of the amorphous phase as evidenced by the A_C/A_A plot, but the much narrower MBM fwhm indicates the presence of crystallites of better quality likely due to the presence of larger and less defected grains.

Moreover, a somewhat opposite behavior is observed in the depositions at 50 and 75 °C. Here, A_C/A_A does not show any significant difference between the two growth rates (similar presence of amorphous phase), while the fwhm of the macrocycle breathing band indicates a better crystalline quality in the samples grown at the highest deposition rate as deduced by the narrower width of the macrocycle breathing band.

It is also interesting to notice that we achieved both the highest and the lowest degree of order for the deposition at 0.05 nm/min (see Figure 8a), pointing to processes that can both increase the film ordering at low temperatures while causing higher disorder at intermediate temperatures. On the other hand, deposition at higher rates seems to attenuate the influence of temperature on the crystalline order, indicating that a high

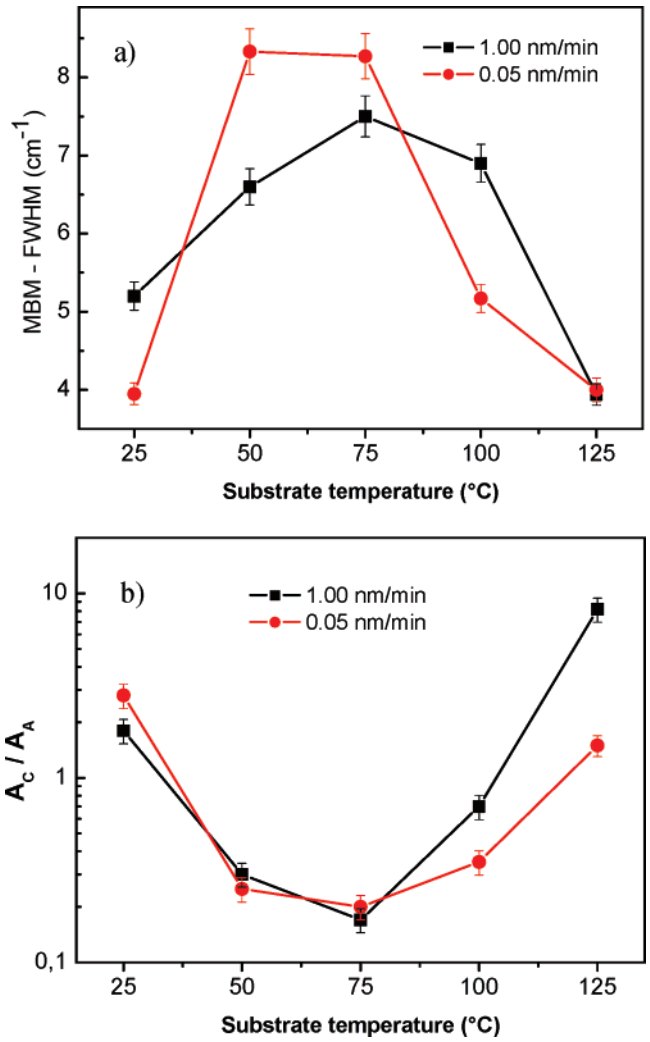

Figure 8. (a) fwhm of the MBM at 678 cm^{-1} as a function of substrate temperature. Width has been averaged over the collected micro-Raman spectra for each sample deposited by SuMBD. (b) Evolution as a function of the temperature of film growth of the ratio between the areas of two pyrrole stretching peaks, respectively, indicating crystalline (A_C) and amorphous (A_A) character (see text).

particle arrival rate is a factor limiting the dynamics of the grain growth by likely modifying molecular diffusion and assembling on the surface.

In fact, several factors affect the growth dynamics of a molecular film, including intermolecular and molecule−substrate interactions, substrate temperature, deposition rate, energy, and momentum of precursors. Once the type of substrate and the arrival rate are fixed, the processes involved in the growth of organic films by OMBD are essentially driven by temperature. Here, we show that in SuMBD, there are other factors playing a decisive role. Kinetic energy of the impinging molecules plays in particular a key role in the development of crystalline structures because it strongly influences the diffusion length on the surface and the critical size for the formation of stable islands. This has been already demonstrated in the growth at room temperature of highly ordered pentacene films,[22] the improved transport properties of which have also been applied in the fabrication of organic field effect transistors.[23] By tuning the kinetic energy, one can control the regime of growth of the first molecular layers that are of fundamental importance in the development of crystalline structures in thin organic films.

From the experiments on TiOPc discussed here, one can envisage a sort of competition between the effects indicated by the substrate temperature and those due to the kinetic energy of the molecules. From this point of view, we can indeed identify three growth regimes associated to as many temperature intervals. Above 100 °C, the data indicate that the processes are essentially driven by temperature since we observe with SuMBD the same properties and trends of conventional low energy evaporation techniques. Between 100 and 50 °C instead, the processes leading to the growth of ordered structures induced by the kinetic energy of the molecule seem to be increasingly quenched or ineffective. Only at room temperature, and below, the contribution of kinetic energy results in the overall development of crystalline phases. This picture is consistent with the consideration that temperature activates and sustains, in the same statistical way depending on the activation energies involved, many different processes such as particle and island diffusion, island reorganization, re-evaporation, etc. On the contrary, the contribution of kinetic energy could be much more selective, as observed also on other molecules such as pentacene.[23] In particular, the diffusion length of the molecules on the surface is enhanced, causing, in a diffusion-limited growth regime, the reduction of the critical nucleus for island nucleation and therefore the growth of less defected and larger molecular crystals.[22,24] In this framework, the substrate temperature can be seen as an interfering factor, modifying the coalescence mechanism between adjacent islands and/or leading to disruption and disordering in the island via re-evaporation.

Conclusion

The growth of TiOPc thin films on quartz has been studied as a function of substrate temperature, exploring the ability to control polymorphisms by supersonic molecular beam growth. Our combined UV−vis absorption and micro-Raman study demonstrates that this is a viable and promising approach. In particular, the growth of polycrystalline films was achieved in temperature ranges where conventional techniques produce only amorphous films. We have shown that the relative abundance of phase I and phase II polymorphs could be controlled by beam parameters to an unprecedented extent. We have demonstrated that the kinetic energy supplied to the molecules by SuMBD plays a key role, confirming results on rod-like molecules on different substrates. We have identified the effects of different regimes of growth, depending on substrate temperature and growth rates, and envisaged a competitive mechanism between substrate temperature and precursor kinetic energy. We have shown that a detailed combined study of optical absorption and micro-Raman spectroscopy is a viable powerful tool for a detailed analysis of the crystalline structure of the films, especially giving information about the contribution of the amorphous phase that cannot be easily obtained by using optical absorption or XRD techniques alone.

Acknowledgment. The authors thank Tiziana Barone for her valuable help in micro-Raman measurements. We acknowledge technical support from C. Corradi and M. Mazzola. We are also very grateful to M. Nardi, R. Verucchi, and L. Aversa for very stimulating discussions. This work was made possible by the financial support of Provincia Autonoma di Trento Project "nanoCOSHy" and of the Italian Ministry of Education, University and Research MIUR−FIRB program projects "SyNERGY" − "RBNE03S7XZ".

References and Notes

(1) Sakaguchi, K.; Chikamatsu, M.; Yoshida, Y.; Azumi, R.; Yase, K. *Jpn. J. Appl. Phys.* **2007**, *46*, 345. Guillaud, G.; Simon, J.; Germain, J. P. *Coord. Chem. Rev.* **1998**, *178−180*, 1433.

(2) Abdeldayem, H. A.; Frazier, D. O.; Penn, B. G.; Smith, D. D.; Banks, C. E. *Thin Solid Films* **1999**, *350*, 245.

(3) Zhou, X. Q.; Wang, M.; Yang, S. L. *Mater. Chem. Phys.* **2002**, *73*, 70. Wang, W. B.; Li, X.; Wang, S.; Hou, W. *Dyes Pigm.* **2007**, *72*, 38.

(4) Zhang, Q.; Wang, D.; Xu, J.; Cao, J.; Sun, J.; Wang, M. *Mater. Chem. Phys*. **2003**, *82*, 525.

(5) Yamaguchi, S.; Sasaki, Y. *Chem. Phys. Lett.* **2000**, *323*, 35.

(6) Nishi, T.; Kanai, K.; Ouchi, Y.; Willis, M. R.; Seki, K. *Chem. Phys.* **2006**, *325*, 121.

(7) Hiller, W.; Strähle, J.; Kobel, W.; Hanack, M. *Z. Kristallogr*. **1982**, *159*, 173.

(8) Mizuguchi, J. *Krist. Technol.* **1981**, *16*, 695.

(9) Oka, K.; Okada, O.; Nukada, K. *Jpn. J. Appl. Phys.* **1992**, *31*, 2181.

(10) Saito, T.; Iwakabe, Y.; Kobayashi, T.; Suzuki, S.; Iwayanagi, T. *J. Phys. Chem.* **1994**, *98*, 2726.

(11) Mizuguchi, J.; Rihs, G.; Karfunkel, H. R. *J. Phys. Chem.* **1995**, *99*, 16217.

(12) Jennings, C. A.; Aroca, R.; Kovacs, G. J.; Hsaio, C. *J. Raman Spectrosc.* **1996**, *27*, 867.

(13) Del Caño, T.; Aroca, R.; De Saja, J. A.; Rodriguez-Mendez, M. L. *Langmuir* **2003**, *19*, 3747.

(14) Yamashita, A.; Maruno, T.; Hayashi, T. *J. Phys. Chem*. **1994**, *98*, 12695.

(15) Brinkmann, M.; Wittmann, J.; Barthel, M.; Hanack, M.; Chaumont, C. *Chem. Mater*. **2002**, *14*, 904.

(16) Saito, T.; Sisk, W.; Kobayashi, T.; Suzuki, S.; Iwayanagi, T. *J. Phys. Chem*. **1993**, *97*, 8026.

(17) Walzer, K.; Toccoli, T.; Pallaoro, A.; Verucchi, R.; Fritz, T.; Leo, K.; Boschetti, A.; Iannotta, S. *Surf. Sci.* **2004**, *573*, 346.

(18) Walzer, K.; Toccoli, T.; Pallaoro, A.; Iannotta, S.; Wagner, C.; Fritz, T.; Leo, K. *Surf. Sci.* **2006**, *600*, 2064.

(19) Toccoli, T.; van Opbergen, M.; Boschetti, A.; Ciullo, G.; Ronchin, S.; Iannotta, S. *Philos. Mag. B* **1999**, *79*, 2157.

(20) Milani, P.; Iannotta, S. *Cluster Beam Synthesis of Nanostructured Materials*; Springer-Verlag; Berlin, 1999.

(21) Toyota, K.; Hasegawa, J.; Nakatsuji, H. *J. Phys. Chem. A* **1997**, *101*, 446.

(22) Wu, Y.; Toccoli, T.; Koch, N.; Iacob, E.; Pallaoro, A.; Rudolf, P.; Iannotta, S. *Phys. Rev. Lett.* **2007**, *98*, 76601.

(23) Toccoli, T.; Pallaoro, A.; Coppedè, N.; Iannotta, S.; De Angelis, F.; Mariucci, L.; Fortunato, G. *Appl. Phys. Lett.* **2006**, *88*, 132106.

(24) Ruiz, R.; Nickel, B.; Koch, N.; Feldman, L. C.; Haglund, R. F., Jr.; Kahn, A.; Family, F.; Scoles, G. *Phys. Rev. Lett.* **2003**, *91*, 136102.